Supplement of Earth Syst. Dynam., 13, 1197–1214, 2022
https://doi.org/10.5194/esd-13-1197-2022-supplement

Earth System Dynamics
Open Access

Supplement of

Present and future European heat wave magnitudes: climatologies, trends, and their associated uncertainties in GCM-RCM model chains

Changgui Lin et al.

Correspondence to: Changgui Lin (mapulynn@gmail.com)

Contents of this file

1. Supplementary text: Understanding the HWMId
2. Figure S1–11
3. Table S1–5

Understanding the HWMId

The HWMId (Russo et al., 2015) used in the study is a fairly established indicator for classifying heat waves, taking into account both the duration and intensity. The detailed definition of HWMId can be found in Sect. 2.1, as well as Russo et al. (2015). It is worth exploring how it works by presenting examples though. Figures S1 and S2 show the spatial distribution of observed (E-OBS) European HWMId values and the detected heat waves at four selected grid points for the years 2007 and 1989, respectively. Following the definition, heat waves are detected when daily maximum temperature exceeds the daily threshold at least three consecutive days, where the threshold for a given day is 90^{th} percentile of daily maximum temperature within the 31-day window centered at this day and within the reference period (1989–2008 for the examples shown here, same as the results in Sect. 3.1). The HWMId value at each grid point is equal to the maximum red area above the climatological 25^{th} percentile of maximum temperature in Fig. S1b (or Fig. S2b) normalized by the climatological interquartile range (IQR) within the reference period, where the 25^{th} percentile and the IQR are constant at a given grid point. As such, the following points are noted:

A) The yearly HWMId values shown on the map may not necessarily represent the spatial distribution of magnitudes of a single heat wave (e.g., occurred in the same period) but the maximum magnitudes of the grid points respectively. For example, Fig. S1b (or Fig. S2b) shows that the heat wave with maximum red areas appeared at different time of the year for the four selected grid points.

B) The yearly HWMId values are in most cases associated with summertime heat waves due to the higher temperature (Fig. S1b and S2b). However, it does not rule out the case that the heat waves with the maximum magnitudes appear in wintertime; an example is given at grid point “SE” in 1989 (Fig. S2b).

C) The HWMId can certainly identify those outrageous heat waves reported by the news headlines according to Russo et al. (2015, Fig. 2 therein). Here, the heat wave occurred over southern Europe in 2017 summer is clearly visualized in Fig. S1a. However, as an index that is reference period-based, the HWMId might be problematical when quantifying magnitudes of moderate heat waves within the reference period, because a higher threshold can be expected for a location with more heat wave activities. Figure S3 shows that the grid point “SE” compared to points in western Europe has a shorter distance between daily 90^{th} and 95^{th} percentiles (within a 31-day window) of daily maximum temperature within 1989–2008, where the former was used as the threshold for the HWMId within Sect. 3.1, over the long summer season (May–September), indicating very likely less heat wave activities at southeastern Europe. Considering that the yearly HWMId values are in most cases associated with summertime heat waves (i.e., Point B), therefore, the result shown in Fig. S1a explains the spatial pattern of HWMId with values in western coastal areas higher than those in eastern areas (Fig. 1a).

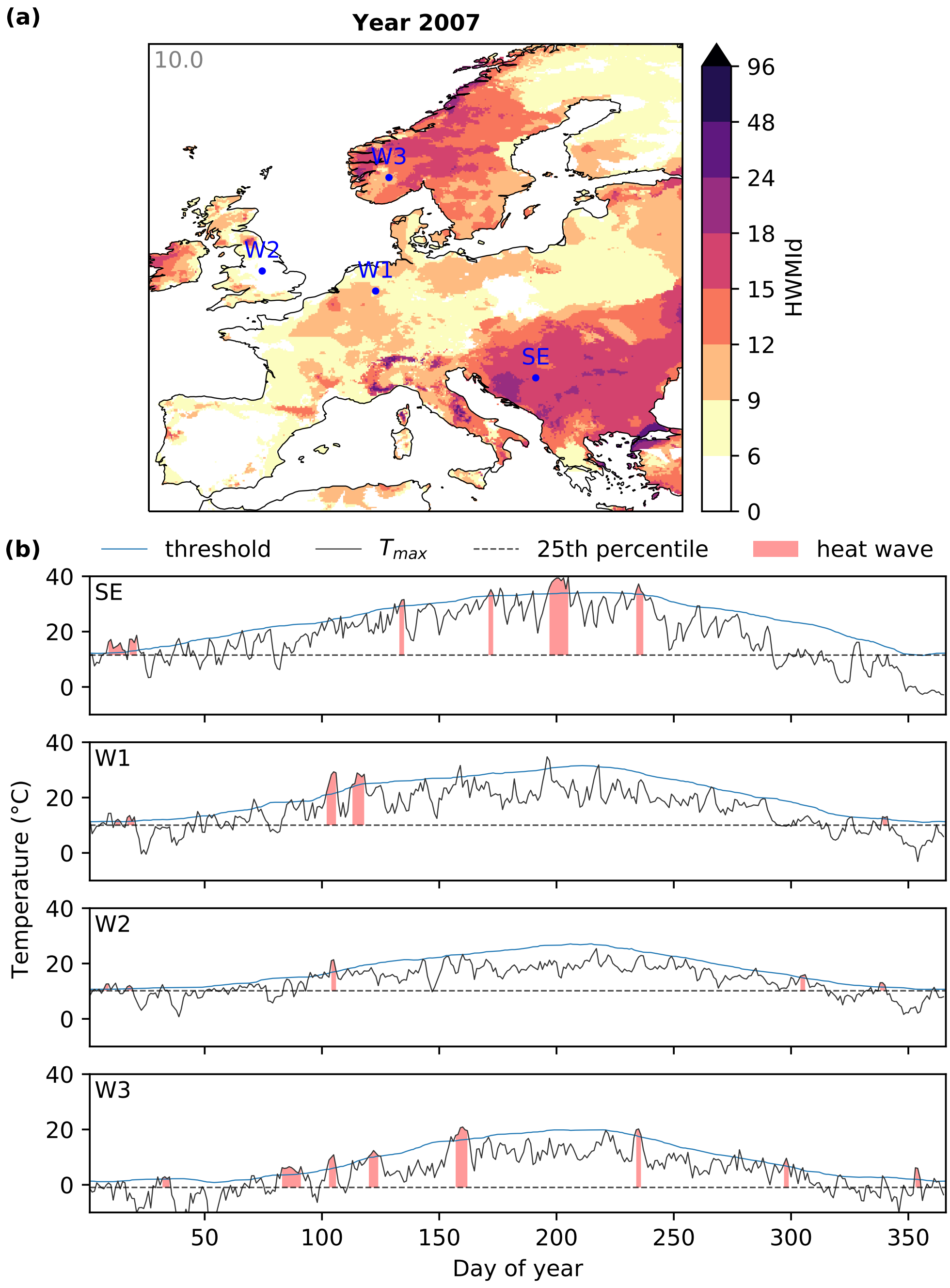

Figure S1. (**a**) Spatial distribution of observed (E-OBS) European HWMId values (with area-weighted average shown in the top-left corner) and (**b**) detected heat waves according to daily maximum temperature and daily threshold at four grid points ("SE", "W1", "W2", and "W3"; with locations respectively labeled in the map in **a**) for the year 2007.

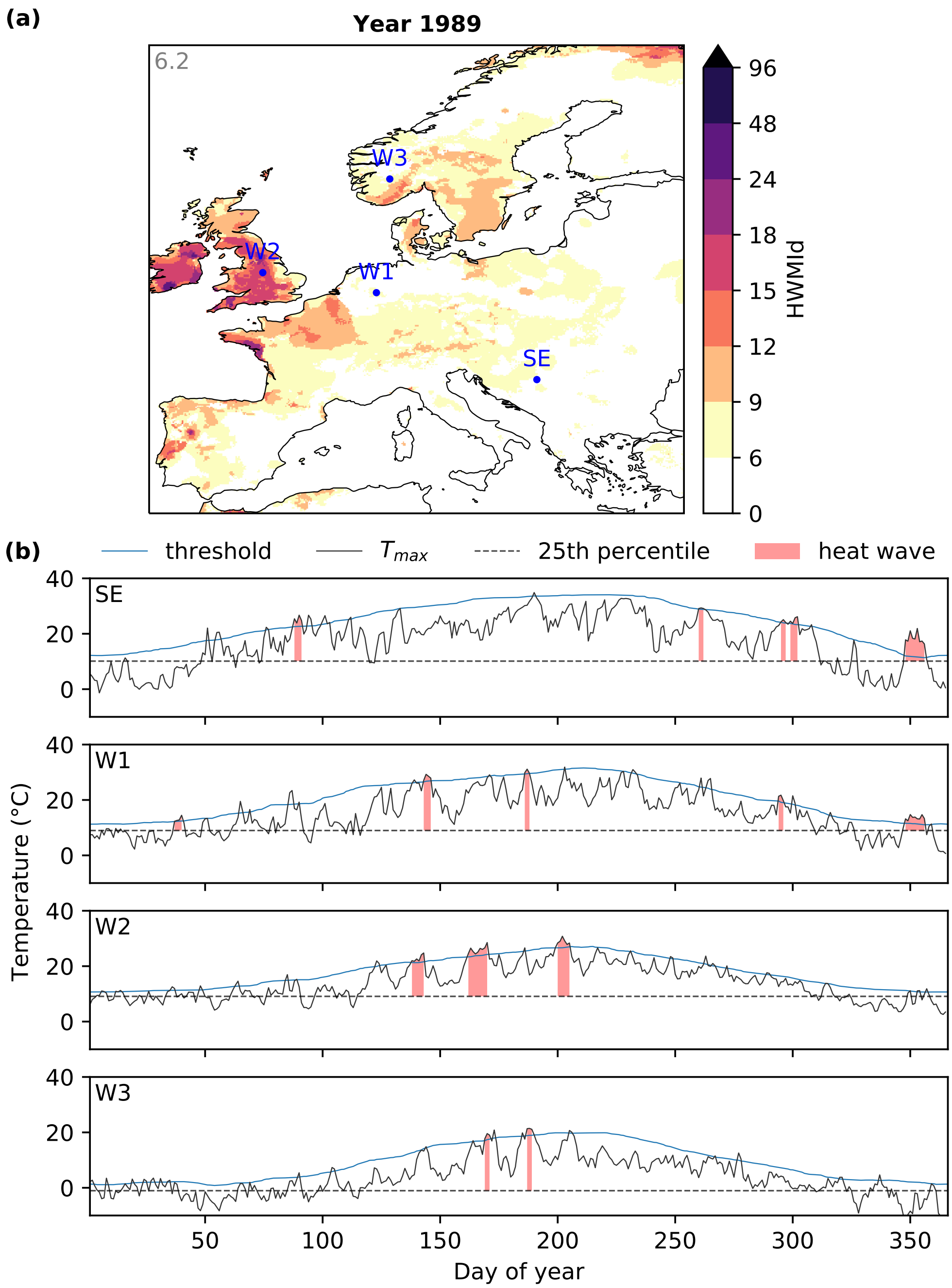

Figure S2. Similar to Fig. S1 but for the year 1989.

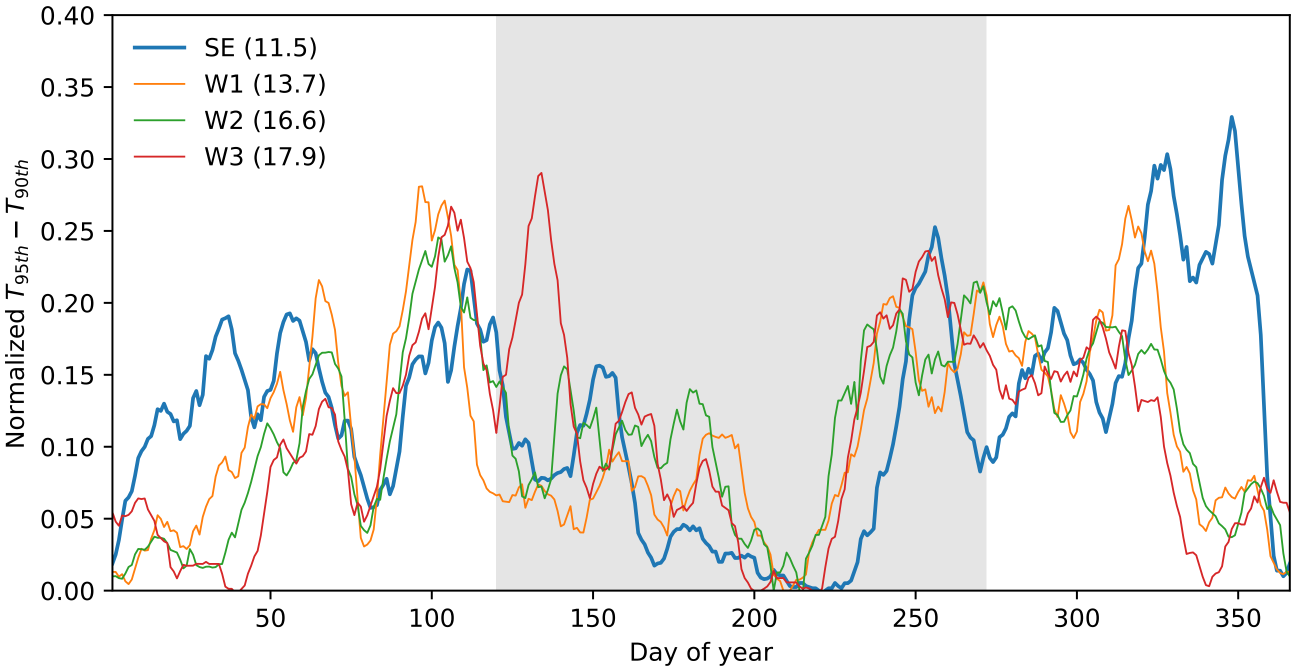

Figure S3. Distance between daily 90th and 95th percentiles (within a 31-day window) of daily maximum temperature within the reference period (1989–2008 here) normalized by the climatological IQR within the same period at four grid points ("SE", "W1", "W2", and "W3"; with locations respectively labeled in the map in Fig. S1a). Numerals in the legend are the sum over the long summer season (May–September; denoted by the gray background).

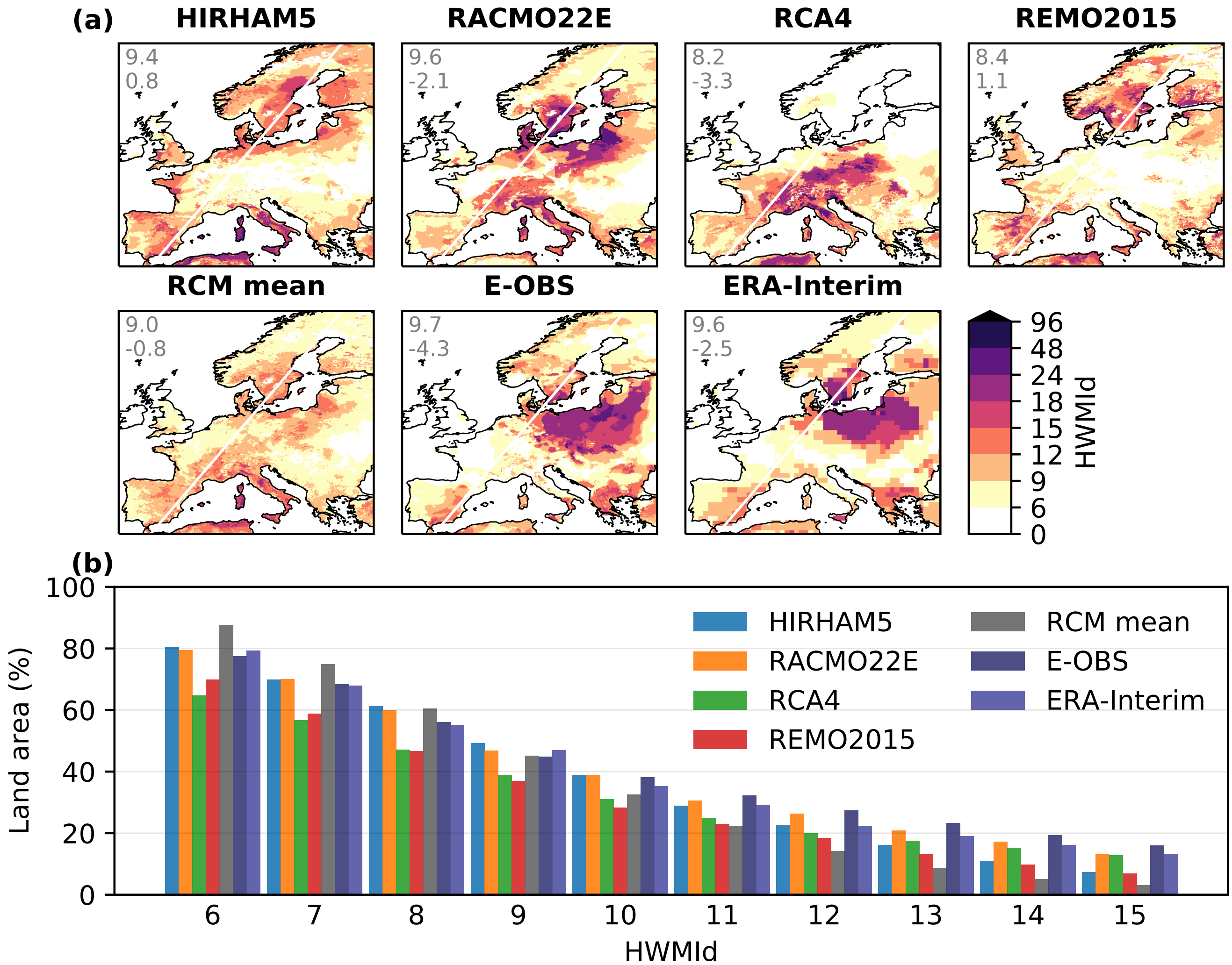

Figure S4. HWMId of the year 1994 in the four RCMs' evaluation runs, the multi-RCM mean, E-OBS, and ERA-Interim: (**a**) spatial pattern, and (**b**) percentage of the land area exceeding certain HWMId levels (6, 7, 8, ..., 15). The two numerals in each map shows the area-weighted average over the entire domain and the difference between western and eastern parts divided by the white line, respectively.

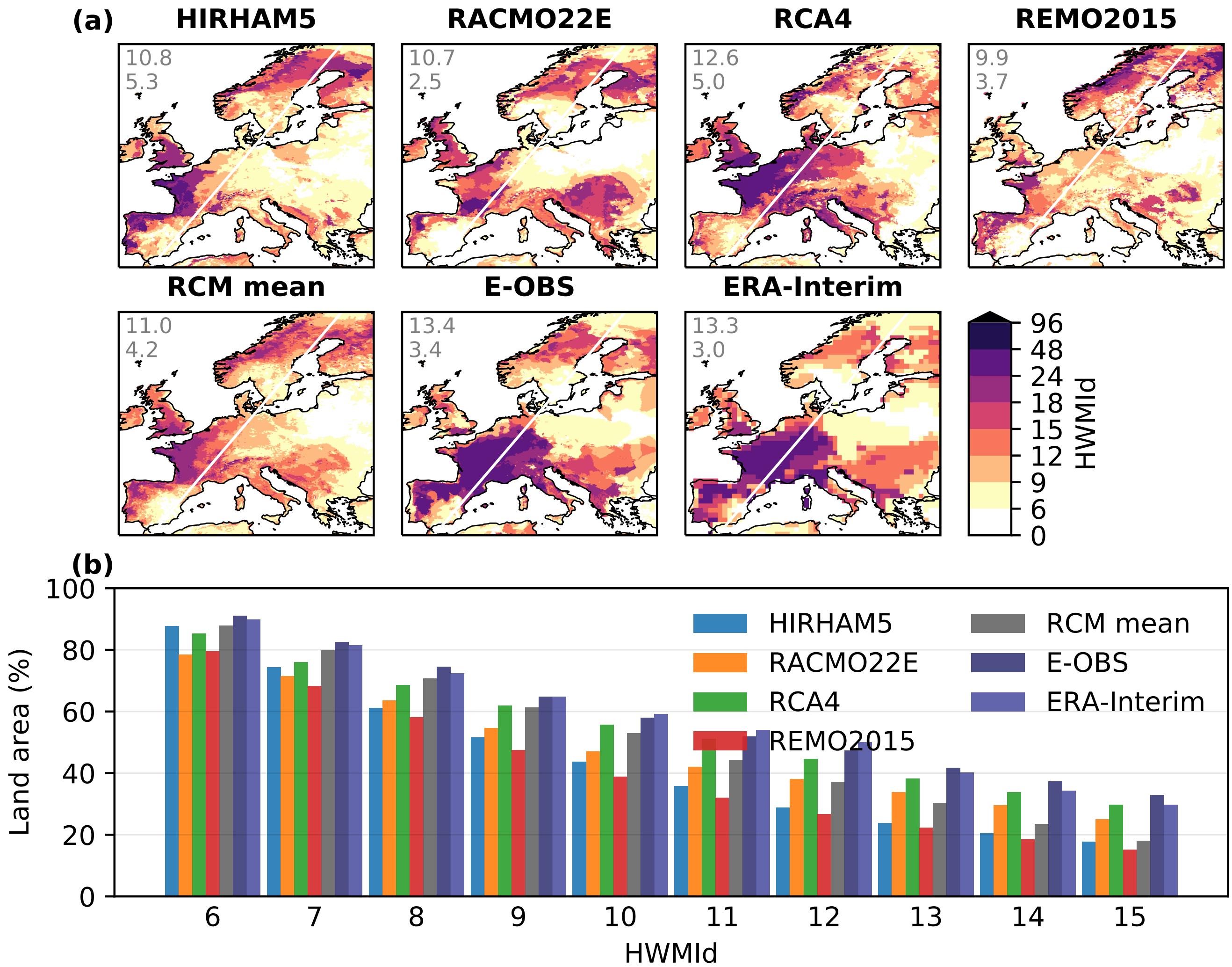

Figure S5. Similar to Fig. S4 but of the year 2003.

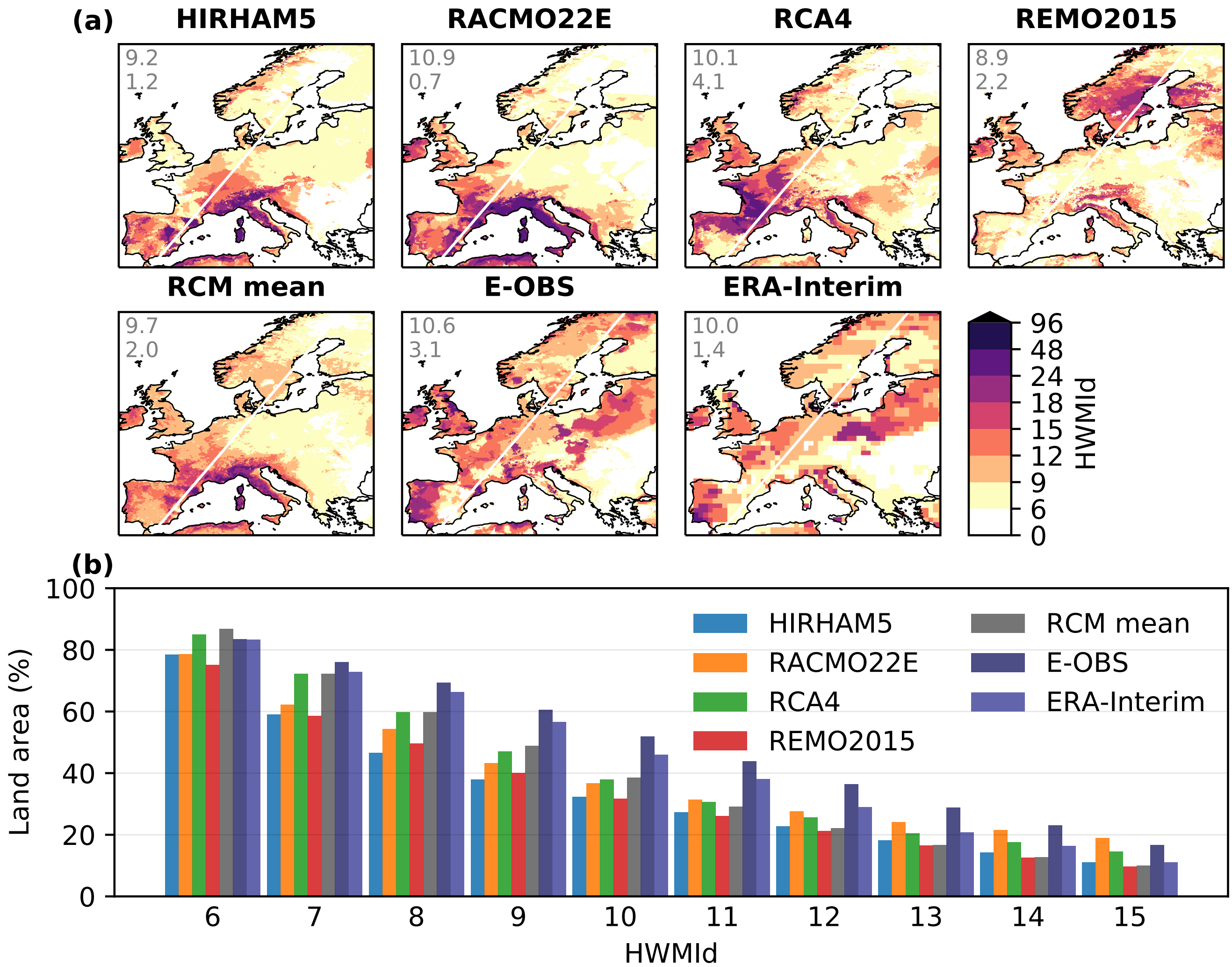

Figure S6. Similar to Fig. S4 but of the year 2006.

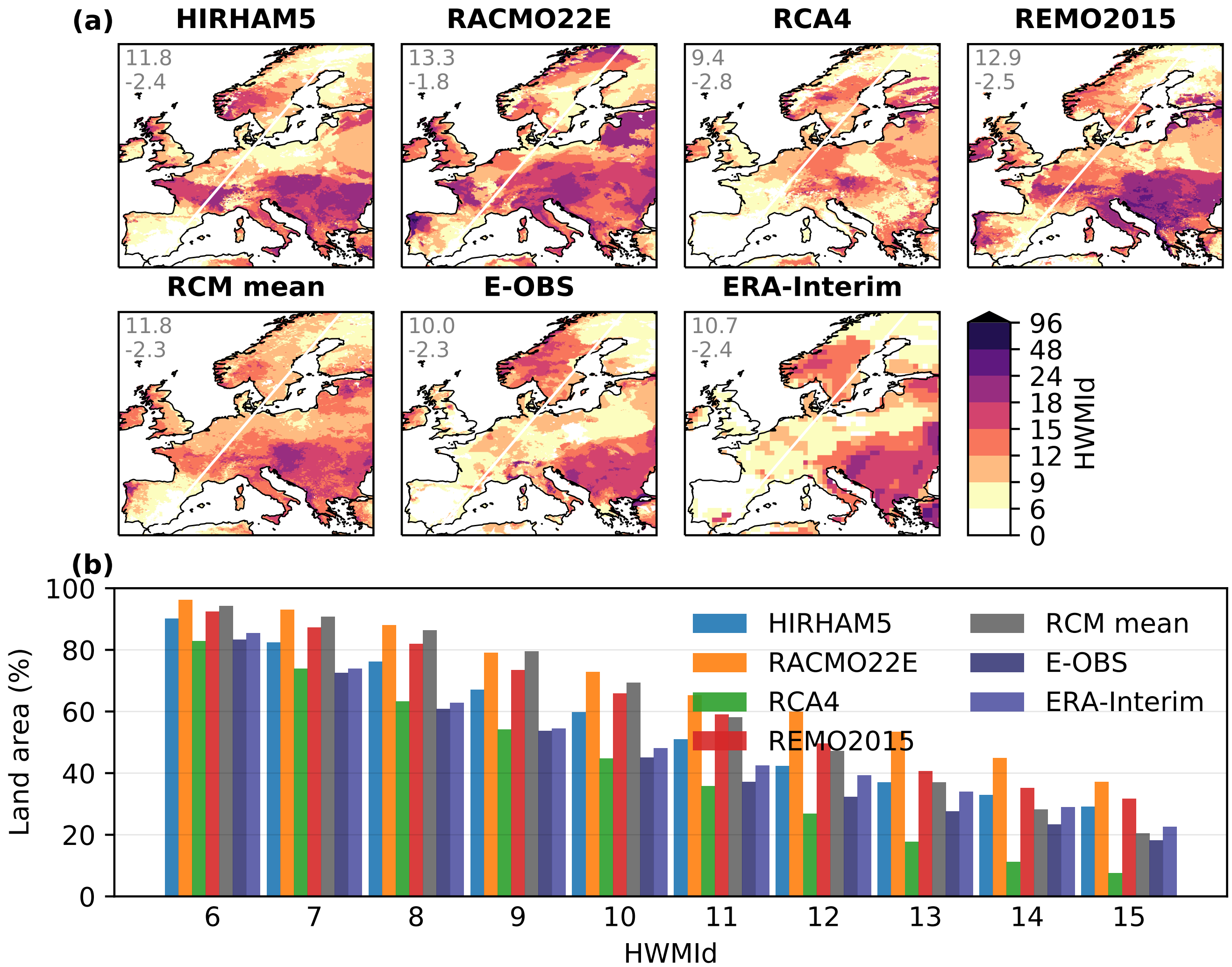

Figure S7. Similar to Fig. S4 but of the year 2007.

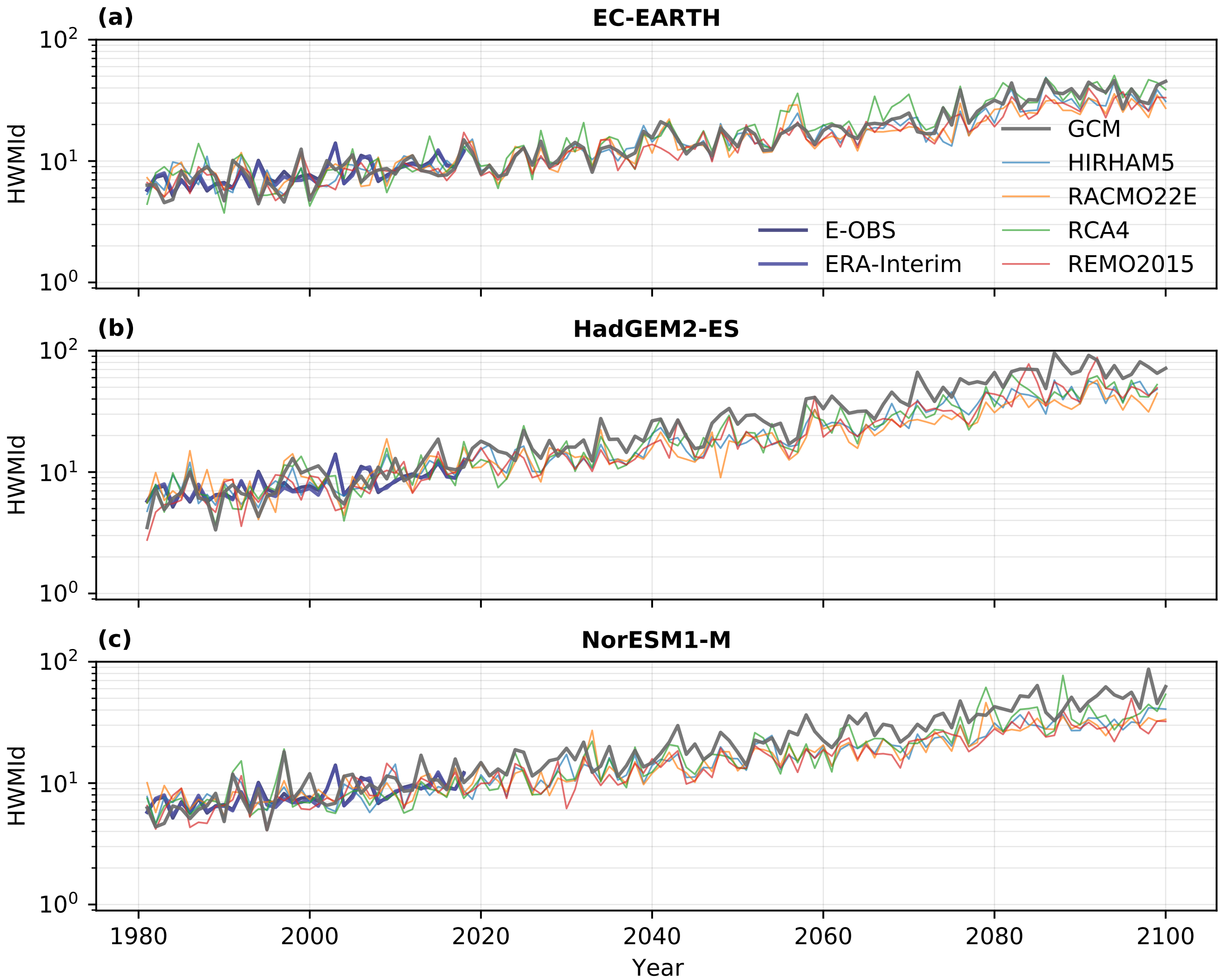

Figure S8. Time series of regional mean HWMId, grouped by the driving GCMs: (a) EC-EARTH, (b) HadGEM2-ES, and (**c**) NorESM1-M. Colors represent different RCMs and gray the GCMs themselves. Data from E-OBS and ERA-Interim are also shown for comparison under the recent past climate. Note that a logarithmic-scale y-axis is used.

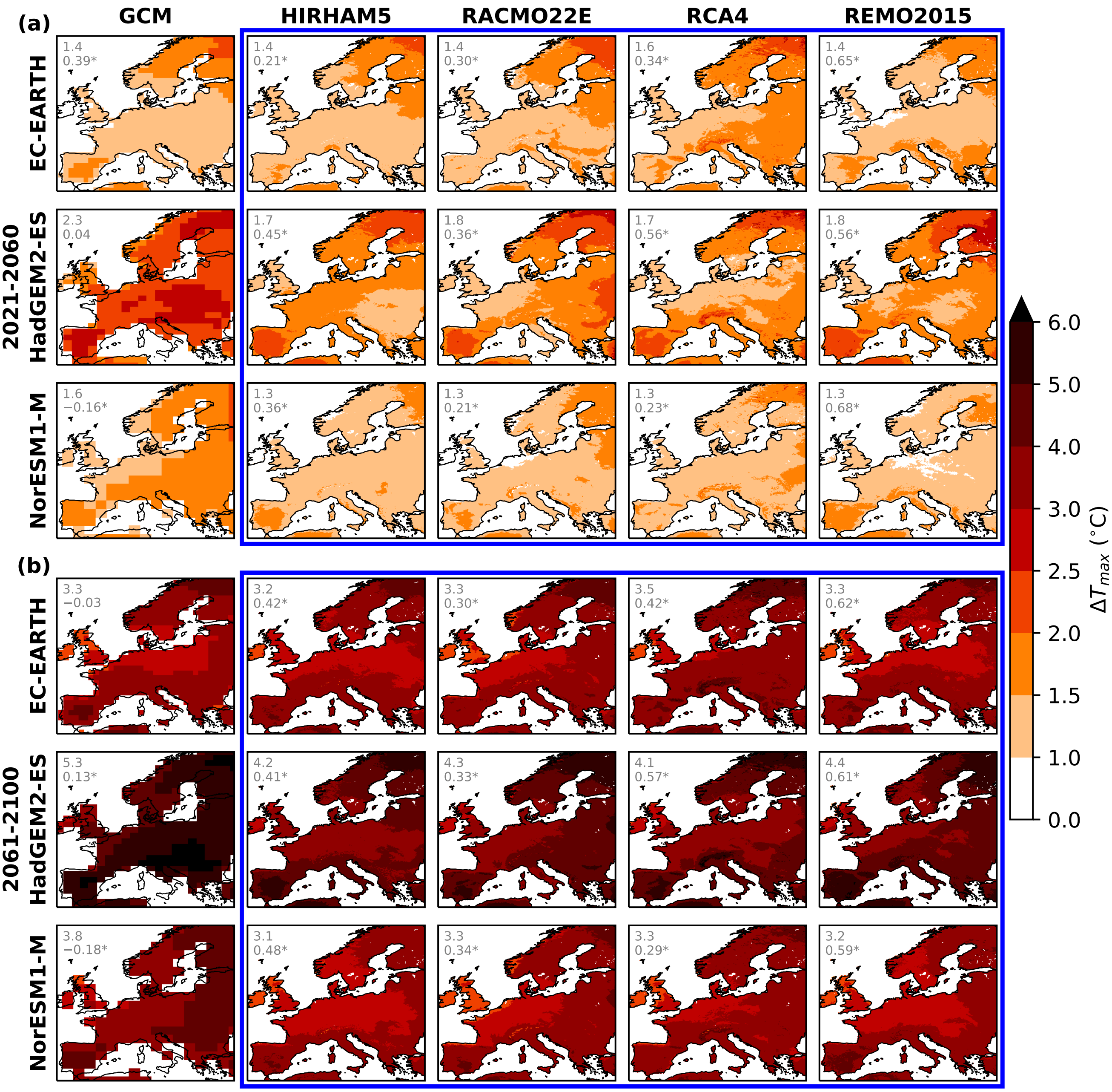

Figure S9. Change in the annual mean of daily maximum temperature in the nearest decades (**a**: 2021–2060) and in the end of the century (**b**: 2061–2100) relative to the recent past climate. The numerals in each map show the area-weighted average and the spatial r with the relevant change in HWMId (with '*' indicating statistically significant at $p < 0.05$).

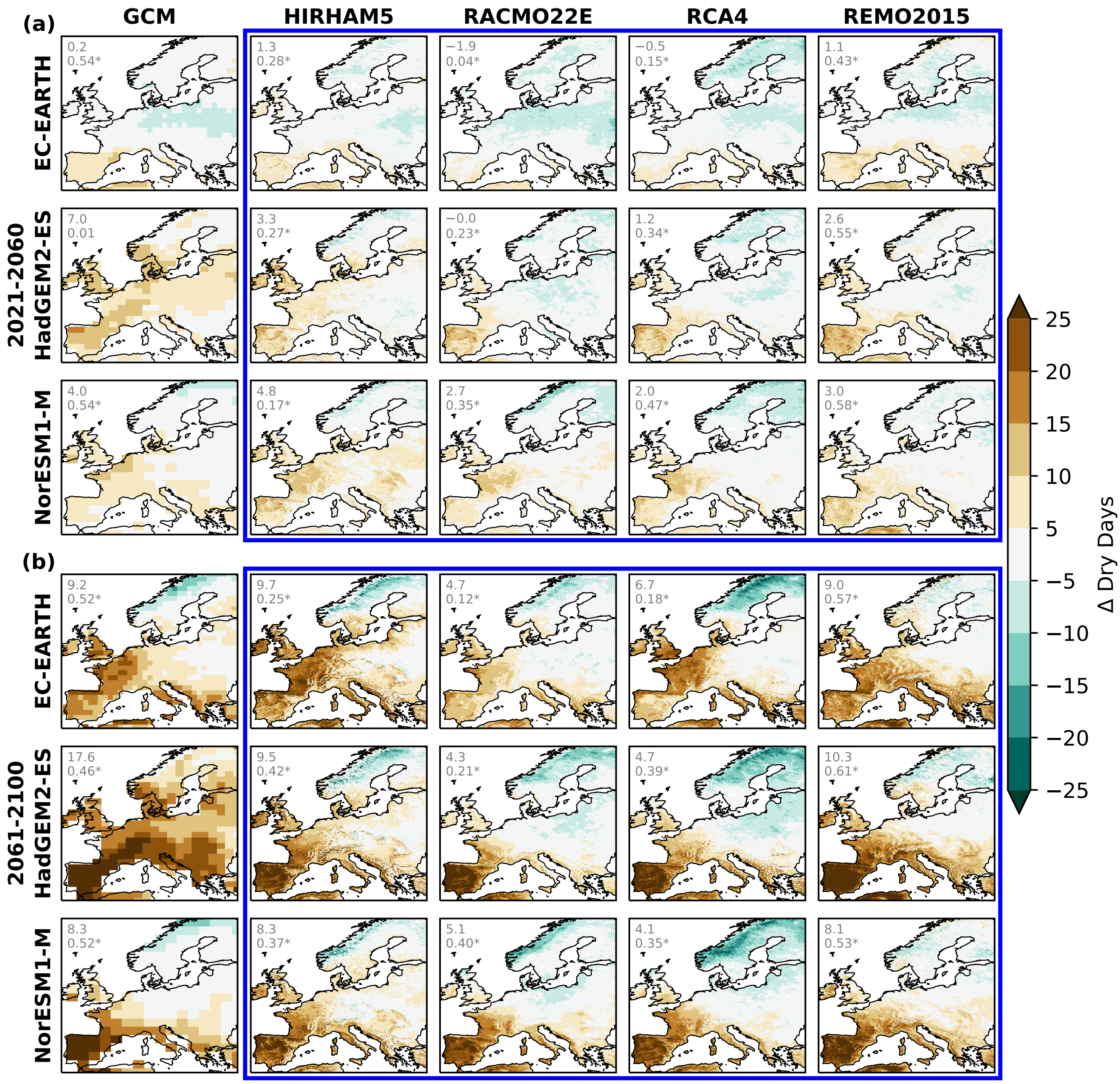

Figure S10. As Fig. S9 but for the change in the annual number of dry days (with precipitation less than 1 mm).

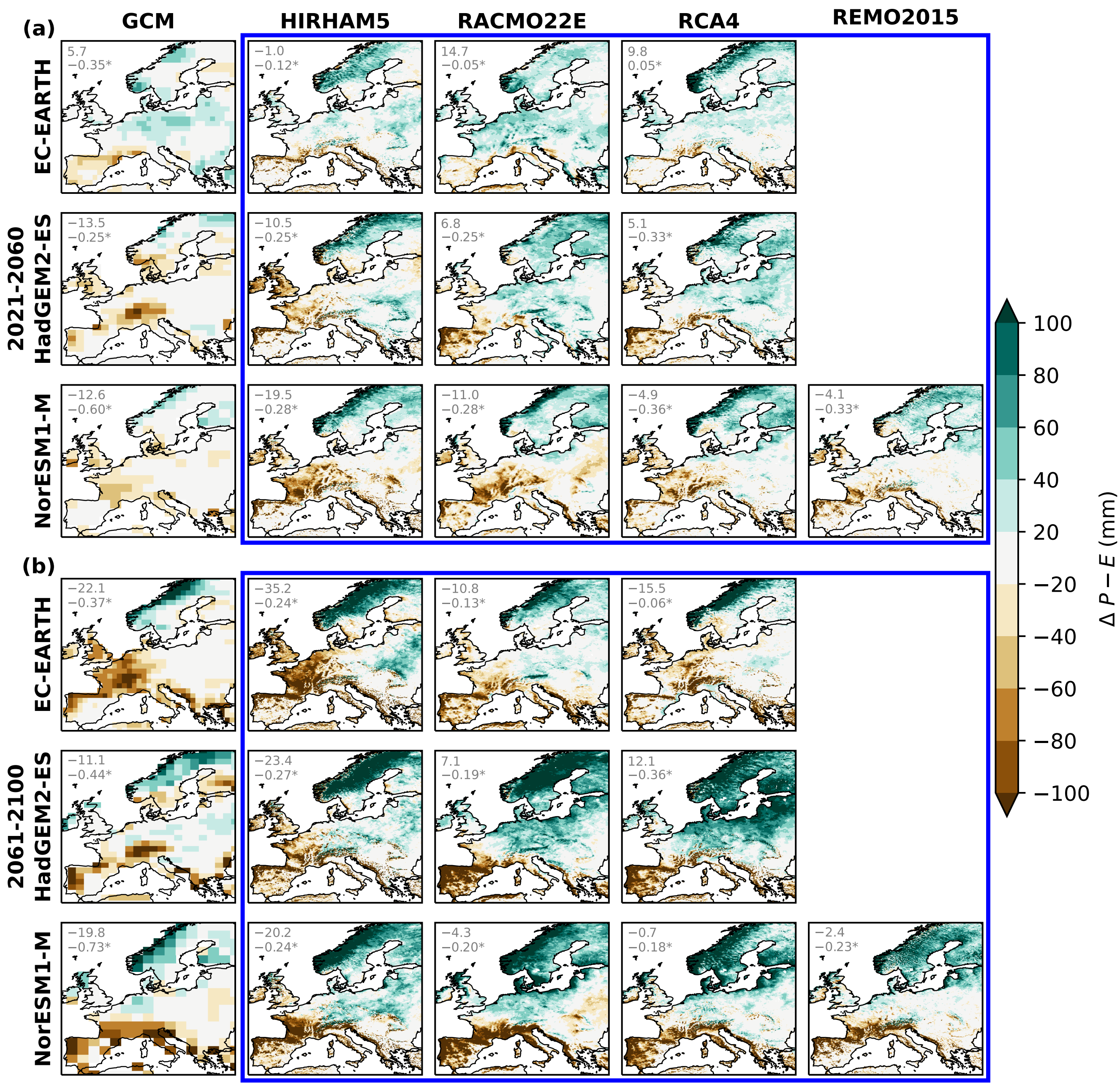

Figure S11. As Fig. S9 but for the change in the annual mean of $P-E$. Due to the missing evaporation data in the simulations of REMO2015 driven by EC-EARTH and HadGEM2-ES, the relevant places are left blank.

Table S1. Spatial RMSE and r for the climatological mean HWMId under the recent past climate (1981–2020). Numbers are given the three pairs of simulations for the GCMs* as well as for each of the four RCMs driven by the three GCMs (i.e., columns of Fig. 3).

	GCM		HIRHAM5		RACMO22E		RCA4		REMO2015	
RMSE:										
	E	H	E	H	E	H	E	H	E	H
H	1.44		0.78		1.13		1.04		0.72	
N	1.57	1.36	0.95	0.92	1.03	1.27	1.11	1.30	0.82	0.79
r^{**}:										
	E	H	E	H	E	H	E	H	E	H
H	0.48		0.86		0.79		0.75		0.78	
N	0.29	0.08	0.65	0.71	0.50	0.51	0.56	0.56	0.68	0.67

* Abbreviations: E for EC-EARTH, H for HadGEM2-ES, and N for NorESM1-M.

** All are statistically significant at $p < 0.01$.

Table S2. Similar to Table S1 but for the ten pairs of simulations (RCM simulations along with their driving GCM simulation) regarding a single driving GCM (i.e., rows of Fig. 3).

	RMSE				r^*			
	GCM	HIRHAM5	RACMO22E	RCA4	GCM	HIRHAM5	RACMO22E	RCA4
EC-EARTH:								
HIRHAM5	1.21				0.35			
RACMO22E	0.92	0.87			0.57	0.71		
RCA4	1.29	0.92	0.90		0.37	0.73	0.71	
REMO2015	1.15	0.80	1.05	1.08	0.30	0.81	0.63	0.68
HadGEM2-ES:								
HIRHAM5	1.42				0.28			
RACMO22E	0.99	1.14			0.58	0.63		
RCA4	1.21	1.00	0.97		0.51	0.65	0.70	
REMO2015	1.50	0.90	1.39	1.25	0.42	0.79	0.72	0.61
NorESM1-M:								
HIRHAM5	1.29				0.56			
RACMO22E	1.14	0.96			0.51	0.50		
RCA4	1.42	0.87	0.92		0.40	0.51	0.53	
REMO2015	1.40	0.76	1.03	0.90	0.61	0.71	0.52	0.49

[*] All are statistically significant at $p < 0.01$.

Table S3. Similar to Table S2 but for the ensemble means and spreads along the GCM dimension (i.e., rows of Fig. 5).

	RMSE				r^*			
	GCM	HIRHAM5	RACMO22E	RCA4	GCM	HIRHAM5	RACMO22E	RCA4
Ensemble mean:								
HIRHAM5	1.03				0.37			
RACMO22E	0.75	0.85			0.58	0.66		
RCA4	0.90	0.76	0.69		0.46	0.68	0.73	
REMO2015	1.09	0.60	0.98	0.85	0.38	0.89	0.70	0.69
Ensemble spread:								
HIRHAM5	1.01				$\underline{-0.02}$			
RACMO22E	1.01	0.78			0.11	0.33		
RCA4	1.21	0.81	0.87		−0.14	0.41	0.30	
REMO2015	1.00	0.65	0.83	0.95	$\underline{-0.02}$	0.20	0.27	0.12

* All apart from those underlined are statistically significant at $p < 0.01$.

Table S4. Spatial MBE, RMSE, and r^* for HWMId values of the years 1994, 2003, 2006, and 2007 in ERA-Interim, the four RCMs' evaluation runs, and the multi-RCM mean (corresponding to Fig. S4– S7, respectively), with E-OBS as reference.

	ERA-Interim	HIRHAM5	RACMO22E	RCA4	REMO2015	RCM mean
1994:						
MBE	−0.30	−0.36	−0.10	−1.50	−1.32	−0.74
RMSE	2.91	6.06	5.13	7.22	6.31	5.06
r	0.83	<u>0.03</u>	0.47	0.11	<u>−0.04</u>	0.27
2003:						
MBE	−0.33	−2.56	−2.73	−0.81	−3.60	−2.43
RMSE	3.05	6.90	6.73	6.00	7.56	5.86
r	0.91	0.44	0.49	0.60	0.33	0.60
2006:						
MBE	−0.54	−1.35	0.30	−0.47	−1.73	0.86
RMSE	3.35	5.49	7.54	5.60	5.19	4.76
r	0.69	0.36	0.23	0.24	0.23	0.36
2007:						
MBE	0.66	1.70	3.28	−0.65	2.86	1.78
RMSE	3.21	4.10	6.05	4.25	5.19	3.79
r	0.77	0.63	0.26	0.41	0.56	0.62

[*] All apart from those underlined are statistically significant at $p < 0.01$.

Table S5. Spatial RMSE and r for the change in the annual mean of daily maximum temperature in the nearest decades (2021–2060) and in the end of the century (2061–2100) relative to the recent past climate (Fig. S9) between each RCM simulation and its driving GCM simulation.

	RMSE				r^*			
	GCM	HIRHAM5	RACMO22E	RCA4	GCM	HIRHAM5	RACMO22E	RCA4
2021–2060:								
EC-EARTH	0.13	0.18	0.27	0.15	0.89	0.85	0.82	0.83
HadGEM2-ES	0.77	0.68	0.76	0.71	0.12	0.34	0.30	0.17
NorESM1-M	0.38	0.33	0.33	0.46	0.60	0.78	0.70	0.36
2061–2100:								
EC-EARTH	0.18	0.30	0.41	0.23	0.92	0.82	0.86	0.88
HadGEM2-ES	1.37	1.20	1.39	1.14	0.47	0.53	0.51	0.58
NorESM1-M	0.86	0.65	0.64	0.75	0.60	0.81	0.71	0.63

[*] All are statistically significant at $p < 0.01$.

References

Russo, S., Sillmann, J., and Fischer, E. M.: Top ten European heatwaves since 1950 and their occurrence in the coming decades, Environmental Research Letters, 10, 124 003, https://doi.org/10.1088/1748-9326, 2015.